

Control of transient enhanced diffusion of boron after laser thermal processing of preamorphized silicon

Y. F. Chong^{a)} and K. L. Pey^{b)}

Department of Electrical and Computer Engineering, National University of Singapore, 4 Engineering Drive 3, Singapore 117576

A. T. S. Wee and T. Osipowicz

Department of Physics, National University of Singapore, Lower Kent Ridge Road, Singapore 119260

A. See and L. Chan

Chartered Semiconductor Manufacturing Ltd., 60 Woodlands Industrial Park D Street 2, Singapore 738406

(Received 25 March 2002; accepted for publication 10 May 2002)

In this article we report the role of excess interstitials in the end-of-range region in transient enhanced diffusion of boron during annealing of laser-processed samples. The results show that although the amorphous layer in preamorphized silicon can be completely annealed by laser irradiation, the end-of-range damages were not sufficiently annealed. The end-of-range region contains a supersaturation of interstitial defects that enhance the diffusion of boron during a post-laser processing anneal. It is found that the transient enhanced diffusion is significantly suppressed when the melt depth is extended beyond the amorphous layer such that the interstitial dose in the region adjacent to the laser-melted layer is minimized. In this way, the abruptness of laser-processed ultrashallow junctions can be maintained upon further annealing at moderately high temperatures. Cross-sectional transmission electron microscopy shows that a virtually defect-free regrown layer is obtained by overmelting beyond the amorphous layer into the substrate. © 2002 American Institute of Physics. [DOI: 10.1063/1.1491278]

I. INTRODUCTION

With the continual scaling of the lateral dimensions of metal–oxide–semiconductor field-effect-transistors (MOS-FETs), the formation of ultrashallow junctions becomes a critical issue in semiconductor processing. Stringent control on the lateral and vertical diffusion of the junctions is necessary to prevent undesirable effects such as punchthrough and short channel effects, which increase the subthreshold leakage current of the devices.^{1,2} Traditionally, junction scaling is achieved using ion implantation and rapid thermal annealing (RTA) with ever-decreasing implantation energies and/or thermal budgets.^{3,4} These approaches, however, have become increasingly complex and do not produce junctions with the ideal box-shaped profiles that can meet the requirements of the international technology road map for semiconductors.⁵ Moreover, during the postimplantation anneal of p^+/n junctions, there is a high tendency that the boron atoms will experience anomalous diffusion (which broadens the dopant profile) due to transient enhanced diffusion (TED),⁶ boron enhanced diffusion,⁷ and oxygen enhanced diffusion.⁸ Fortunately, TED of boron (in the absence of a preamorphized layer) is almost eliminated by reducing the implantation energy to the sub-keV regime such that there is a corresponding increase in the annihilation of implantation-induced interstitials at the silicon surface.⁹

One proposed approach for circumventing some of these problems is the use of laser thermal processing (LTP), which has a “near-zero” thermal budget and is able to form highly activated and abrupt ultrashallow junctions.¹⁰ The LTP process typically involves the preamorphization of the silicon surface by implanting Ge^+ or Si^+ , followed by the melting of the amorphized regions without melting the underlying substrate.^{10,11} This can be achieved because amorphous silicon ($a\text{-Si}$) melts at a temperature that is 200 ± 50 °C lower than the melting point of crystalline Si ($c\text{-Si}$).¹² In this way, a process margin is created since there is a $\sim 15\%$ fluence window whereby the melt depth does not increase further with an increase in fluence.¹¹ Thus the final junction depth would be defined by the preamorphization depth. However, there are some concerns on the formation of extended defects after laser melting and recrystallization.^{13,14} After the preamorphizing implantation (PAI), where the ion implantation dose is sufficiently high to produce a continuous amorphous layer, there exists a highly damaged region in the crystalline material just beyond the amorphous/crystalline (a/c) interface. It is well-established that this end-of-range (EOR) damaged region contains a supersaturation of interstitial point defects created during implantation.¹⁵ During subsequent thermal annealing, these interstitials are released and diffuse toward the surface and into the substrate, and may precipitate into type II extended defects.¹⁶ This release of excess interstitials during annealing causes the enhanced diffusivity of dopant atoms (such as B and P) which diffuse either principally or in part by an interstitial(cy) mechanism in silicon.⁸ Previous studies have shown that the density of

^{a)}Electronic mail: engp9489@nus.edu.sg

^{b)}Present address: School of EEE, Nanyang Technological University, Nanyang Avenue, Singapore 639798.

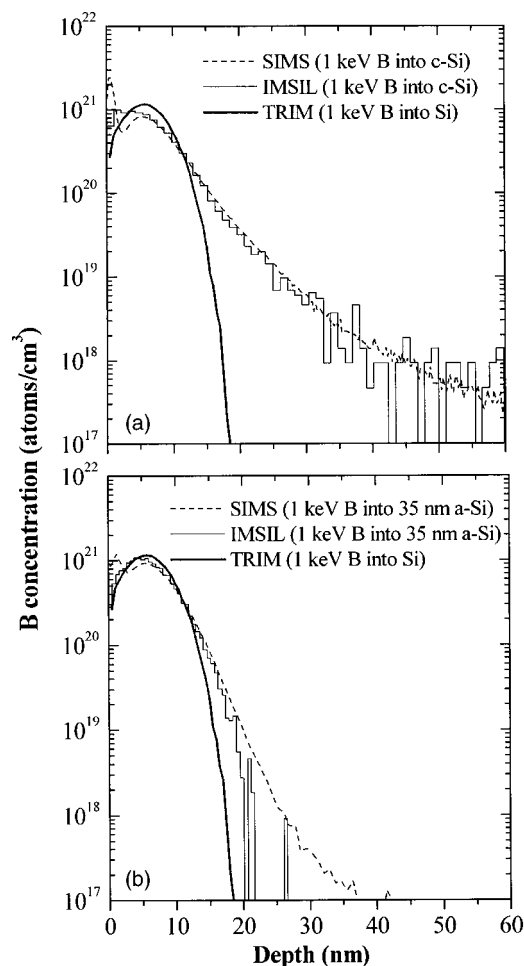


FIG. 1. Comparison of as-implanted 1 keV boron profiles obtained from SIMS with simulated profiles from IMSIL and TRIM. (a) in crystalline Si and (b) in amorphous Si.

defects after LTP can be reduced by optimizing the dose rate of the PAI or by performing a very low temperature anneal prior to LTP to smoothen the *a/c* interface.¹⁴ In this article we report the role of the excess interstitials in the EOR region in the transient enhanced diffusion of boron during a post-LTP anneal. A method based on melting beyond the amorphous layer during the initial LTP step was found to be effective in controlling boron TED during a post-LTP anneal.

II. EXPERIMENT

Ultralow energy $^{11}\text{B}^+$ implantation was performed on 200 mm *n*-type Si (100) wafers at 1 keV to a dose of $1 \times 10^{15}/\text{cm}^2$. Prior to B^+ implantation, the wafers were preamorphized with either Si^+ or Ge^+ implantation. Si^+ was implanted at 10 keV to a dose of $3 \times 10^{15}/\text{cm}^2$ to produce an amorphous layer ~ 350 Å thick. Ge^+ was implanted at 5 keV to a dose of $1 \times 10^{15}/\text{cm}^2$ to produce an amorphous layer ~ 116 Å thick. The samples were then irradiated with a 248 nm KrF laser with a pulse duration of approximately 23 ns. Dopant profiles were analyzed by secondary ion mass spectrometry (SIMS) using a Cameca IMS 6f instrument. A primary beam of O_2^+ ions with a beam current of 20 nA and a net energy of 1 keV was scanned over an area of $250 \times 250 \mu\text{m}^2$. The primary ions impinged upon the surface at an in-

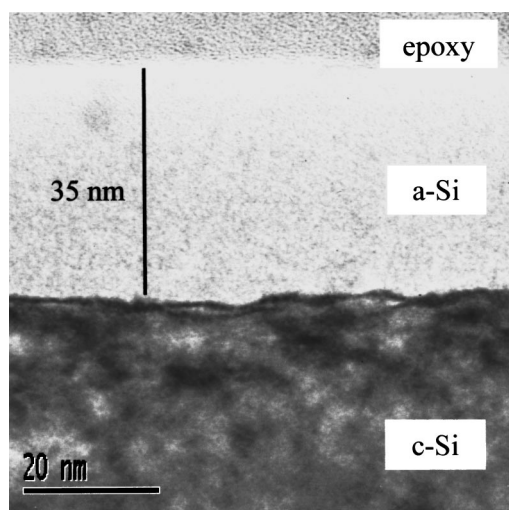


FIG. 2. Cross-sectional transmission electron micrograph of a sample that was preamorphized with $3 \times 10^{15}/\text{cm}^2$, 10 keV Si^+ .

cident angle of 56° , with respect to the surface normal. Secondary ions were collected from the central region ($30 \mu\text{m}$ in diameter) of the sputtered crater. Samples for cross-sectional transmission electron microscopy (XTEM) were prepared by standard procedures such as polishing and subsequent ion milling. The XTEM images were obtained using a transmission electron microscope operating at 200 kV. Rutherford backscattering spectrometry (RBS) was carried out using 2 MeV He^+ ions and backscattered particles were detected at a scattering angle of 160° . Channeling RBS was performed by aligning the incident beam with the $\langle 100 \rangle$ axis of silicon. In this work, simulations of detailed implantation cascades were performed with the Monte Carlo simulator, transport of ions in matter (TRIM),¹⁷ and the binary collision code implant simulator (IMSIL).¹⁸

III. RESULTS AND DISCUSSION

A. Validation of IMSIL

In order to check the validity of the binary collision code IMSIL, we compare the as-implanted boron profiles in *c*-Si and *a*-Si that were obtained from SIMS with simulated profiles from IMSIL and TRIM (Fig. 1). In all cases, the tilt angle and the dose of the boron ion implantation is 0° and $1 \times 10^{15}/\text{cm}^2$, respectively. For the simulation of a 1 keV B^+ implant into *a*-Si using IMSIL, the thickness of the *a*-Si layer on *c*-Si was assigned to be 350 Å. This corresponds approximately to the thickness of the amorphous layer created by the $3 \times 10^{15}/\text{cm}^2$, 10 keV Si^+ PAI (refer to Fig. 2). It should be noted that the TRIM profiles in Figs. 1(a) and 1(b) are the same since there is no option to specify the crystallinity of the substrate in TRIM. In order to have a better fit of the IMSIL results with the actual SIMS profile, a native oxide layer (17 Å thick) was taken into account for the simulation of 1 keV B^+ implantation into (100) *c*-Si. From Fig. 1, it is clear that the shapes of the IMSIL “profiles” (histograms) resemble closely that of the experimental SIMS profiles for both *c*-Si and *a*-Si substrates. On the other hand, the TRIM profile drops off sharply at a depth of $\sim 2.2R_p$, probably due to the

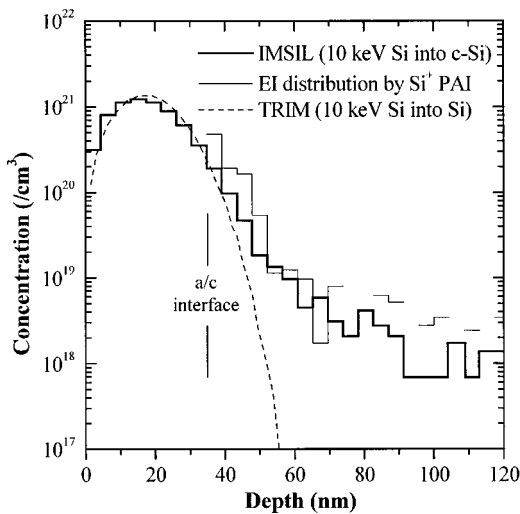


FIG. 3. Simulated profiles of the distribution of ions and excess interstitials for the $3 \times 10^{15}/\text{cm}^2$, 10 keV Si^+ PAI (as obtained from IMSIL and TRIM).

fact that the simulation code for TRIM is applicable only to amorphous targets or random directions of a crystalline target.¹⁹ The excellent agreement between the simulated and measured profiles for the 1 keV B^+ implant validates the use of IMSIL for the simulation of collision cascades during ion implantation into silicon.

B. Simulations of implantation cascades

In light of the previous section, we used IMSIL to simulate the detailed implantation cascades of the $3 \times 10^{15}/\text{cm}^2$, 10 keV Si^+ PAI into *c*-Si, and the results are shown in Fig. 3. The net profile of the excess interstitials (EI) is obtained by subtracting the total number of vacancies from the total number of interstitials that were generated during implantation. It can be seen that the EI profile mimics the simulated as-implanted Si profile, suggesting that the distribution of interstitials somewhat follows the “+1” model, where it is assumed that each implanted ion gives rise to one excess interstitial during annealing.²⁰ As a comparison, the Si ion distribution profile obtained from TRIM is also included in Fig. 3. As expected, there is a discrepancy between the IMSIL and TRIM profiles, especially near the tail of the implant. Since the PAI layer covers the entire boron profile, it is generally accepted that the “vacancies” and “interstitials” that were generated by the 1 keV B^+ implant do not really exist in the amorphous layer. However, the distribution of excess interstitials induced by the boron implantation can still be extracted from IMSIL, and it is found that these EI are confined within the amorphous layer. Hence, for this sample, the excess interstitials in the EOR region that will affect boron TED during the post-LTP RTA is solely contributed by the Si^+ implantation.

C. Enhanced diffusion of boron during post-LTP RTA

Figure 4 shows the SIMS depth profiles of boron after LTP at different fluence and after a post- $0.6 \text{ J}/\text{cm}^2$ LTP RTA at 825°C for 30 s. The thermal budget of this RTA is similar to that of a conventional silicidation process in MOSFET

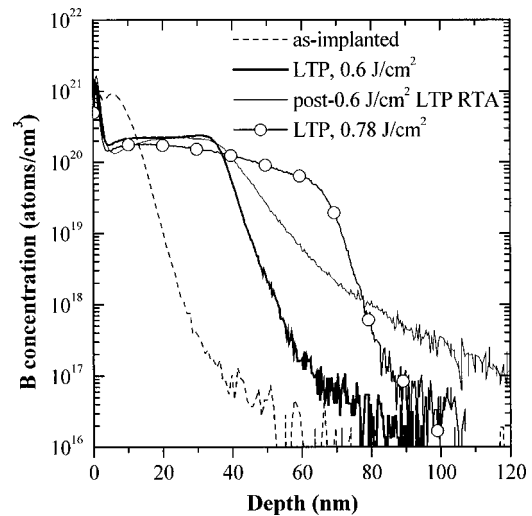


FIG. 4. SIMS depth profiles of boron after LTP at different fluence and after a post-LTP (at $0.6 \text{ J}/\text{cm}^2$) anneal. Transient enhanced diffusion of boron is observed after the post-LTP anneal. The preamorphizing condition was $3 \times 10^{15}/\text{cm}^2$, 10 keV Si^+ .

fabrication. It can be observed that near step-like dopant profiles are obtained directly after LTP. This is due to the melting of the surface regions by the laser irradiation. Since the liquid-phase diffusivity of B in Si is about eight orders of magnitude higher than its solid state diffusivity,¹⁰ the boron atoms diffuse to the maximum melt depth instantaneously to form an abrupt junction. The slight deviation from abrupt junction behavior in Fig. 4 can be attributed to three factors: (i) limited depth resolution of the SIMS instrument, (ii) spatial inhomogeneity of the laser beam, and/or (iii) a nonabrupt *a/c* interface that was created by the Si^+ PAI. The junction depth is thus regarded as the maximum melt depth, which can be defined as the depth that marks a drastic change in the slope of the concentration profile; this corresponds to $\sim 362 \text{ \AA}$ in Fig. 4. The result indicates that the melt front had propagated through the entire amorphous layer, stopping at the original *a/c* interface.

However, when this sample is subjected to a post-LTP anneal at 825°C for 30 s, there is an appreciable shift in the boron profile (Fig. 4). For example, at a concentration of $1 \times 10^{18}/\text{cm}^3$, the junction depth has shifted inward by $\sim 260 \text{ \AA}$ after RTA. This corresponds to a diffusion length ($\sqrt{2Dt}$) that greatly exceeds the equilibrium diffusion length of $\sim 8 \text{ \AA}$ predicted using Fair's value for the intrinsic diffusivity of boron.²¹ The source of this anomalous diffusion is the supersaturation of interstitials in the EOR region. By integrating the EI profile in Fig. 3 (for the region $\sim 200 \text{ \AA}$ beyond the preamorphization depth), the dose of interstitials in the EOR region is calculated to be $\sim 3.9 \times 10^{14}/\text{cm}^2$. At this dose, according to the “phase diagram” for {311} behavior by Stolk *et al.*,⁶ {311} defects and EOR loops are expected to be formed during the initial (ramp-up) stage of the annealing process. Upon further annealing, the unstable {311} defects dissolve while the EOR loops grow into more stable structures. When the {311} defects dissolve, they release excess interstitials for TED. However, TED of boron has been observed to occur in the absence of {311} defects,²² so there

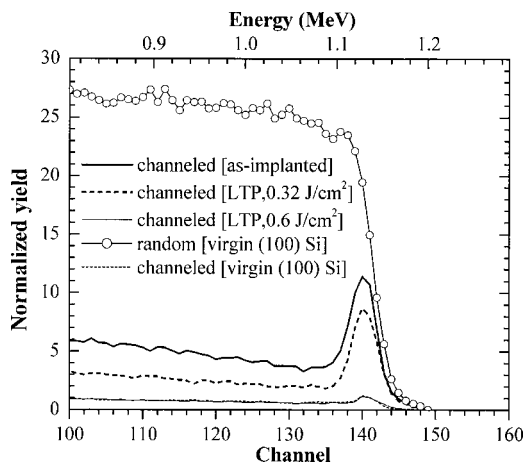


FIG. 5. Random and channeled backscattering spectra of a virgin (100) silicon sample and the Si⁺ preamorphized sample before and after laser annealing.

may be more than one source of interstitials for boron TED. At this moment, a detailed understanding of the evolution of defects during a post-LTP anneal is still lacking.

D. Recrystallization of the preamorphized layer

The channeled backscattering spectra of the Si⁺ preamorphized sample before and after laser annealing are shown in Fig. 5. The random and channeled backscattering spectra of a virgin (100) silicon sample are also shown for reference. The random spectra of the preamorphized and laser-annealed samples are almost identical to that of the virgin sample and are not shown. From Fig. 5 it can be seen that the intensity of the silicon surface peak for the preamorphized sample is greater than that of virgin (100) silicon, indicating the presence of substantial damage in the surface regions of the preamorphized sample. However, there is a reduction in the intensity of the Si surface peak for the preamorphized sample after a low-fluence anneal at 0.32 J/cm². This reduction becomes more significant when the sample was exposed to laser irradiation at 0.6 J/cm². In fact, the channeled RBS spectrum for the latter sample virtually coincides with the spectrum for the virgin sample, indicating that the preamorphized layer has been completely annealed with a single-pulse laser anneal at 0.6 J/cm².

The extent of recrystallization can be determined by computing the value for the minimum yield, χ_{min} , which is the ratio of the integral of the channeled spectrum to the integral of the random spectrum.²³ In this case, the area under consideration is the area under the curve between channel 120 and 130 (Fig. 5). As evident from Table I, the χ_{min} of the 0.6 J/cm² laser-annealed sample is comparable to that of virgin (100) Si substrate, revealing that the amorphous layer has indeed recrystallized to single crystalline (100) Si. However, it should be mentioned that this laser-regrown layer may contain residual defects such as microtwins and stacking faults¹³ that are not detected by RBS. Similarly, EOR defects cannot be easily detected using this technique. Hence, although the preamorphized layer was completely an-

TABLE I. Calculated χ_{min} values for the as-implanted sample, laser-annealed samples, and the virgin silicon sample.

Sample	χ_{min} (%)
Preamorphized	20.54
After LTP at 0.32 J/cm ²	10.95
After LTP at 0.6 J/cm ²	3.32
Virgin (100) Si	3.43

nealed, the EOR damages were not sufficiently annealed by the nanosecond laser irradiation (as indicated by the boron TED during the post-LTP anneal).

E. Control of boron TED during post-LTP anneal

In order to suppress boron TED during post-LTP annealing, it may be necessary to extend the melt depth to beyond the amorphous layer (overmelting) such that the interstitial dose in the region adjacent to the laser-melted layer is minimized. We term this region as the “next to end-of-range” (NEOR) region (refer to Fig. 6). Preferably, the EI dose in the NEOR region (defined as ~200 Å beyond the melt depth) should be less than the threshold dose for {311} formation, which is ~5 × 10¹²/cm².²⁴ From the process margin standpoint, overmelting into the substrate is rather undesirable but this is one alternative to minimize TED after LTP.

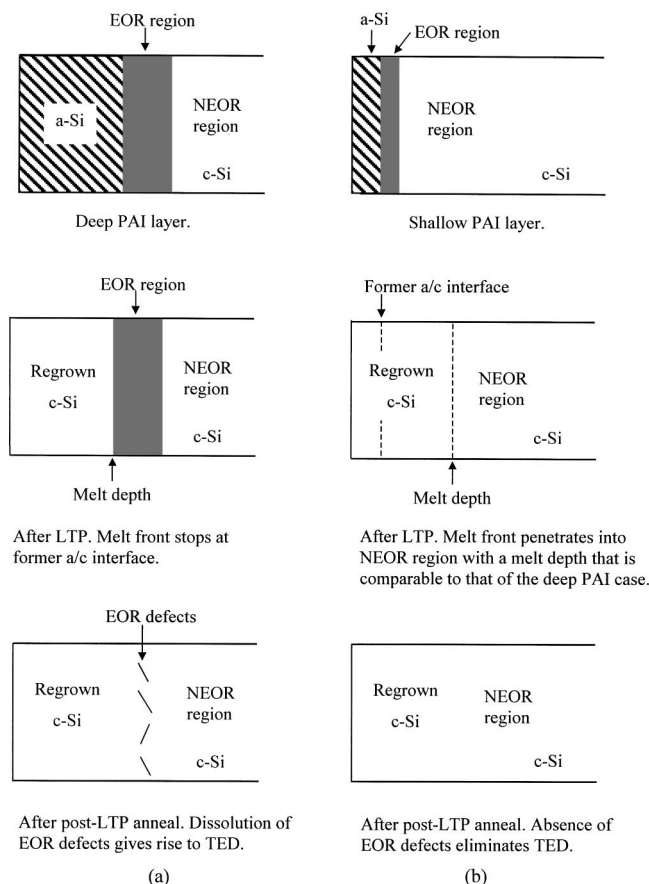


FIG. 6. Schematics showing the effect of melt front position on TED caused by EOR defects. (a) Melt front stops at the former a/c interface. (b) Melt front penetrates into the NEOR region.

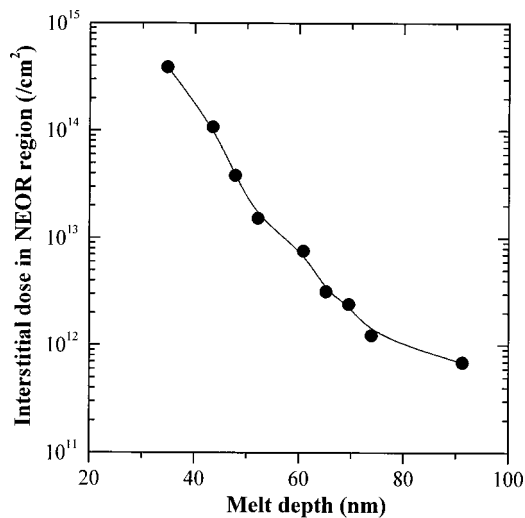


FIG. 7. Plot of the simulated interstitial dose in the NEOR region (for the 10 keV Si⁺ PAI sample) as a function of melt depth.

This is because EOR damage cannot be avoided if a PAI is performed. It is important to note that the melt depth can still be controlled primarily by the laser fluence. Figure 7 is a plot of the simulated interstitial dose in the NEOR region (for the 10 keV Si⁺ PAI sample) as a function of melt depth. It is assumed that the laser-melted Si recrystallizes into a good-quality crystal such that the excess interstitials (if any) trapped in the regrown crystal do not have a significant influence on the boron TED during subsequent anneal. Figure 7 shows that the laser needs to melt at least 630 Å of Si to achieve an EI dose less than $5 \times 10^{12}/\text{cm}^2$ in the NEOR region. This would result in a concentration profile similar to that of the 0.78 J/cm² laser-processed sample shown in Fig. 4. Unfortunately, such a deep junction may have adverse effects on the performance of short-channel devices. Moreover, it can be seen from Fig. 4 that after LTP, there is a slight decrease in boron concentration at the maximum melt depth. The boron atoms are not uniformly distributed within the melted layer due to the insufficient melt duration during LTP.

Therefore we propose to use a PAI of a lower dose and/or implantation energy to produce a shallower amorphous layer to control TED without compromising the final junction depth. Preamorphization of silicon is still necessary in order to prevent channeling (as evident from Fig. 1) and to lower the threshold laser fluence that is required to melt the Si substrate. The second point is illustrated in Fig. 8, where the simulated ratio of the threshold fluence (E_{th}) needed to melt the *a*-Si surface or *c*-Si just beneath the PAI layer to the threshold fluence required to melt *c*-Si alone (E_{melt}) is plotted against preamorphization depth. These results were obtained using a laser melting simulation program.²⁵ For a PAI depth of 116 Å, the E_{th} needed to melt the *a*-Si surface is reduced by ~40% while the E_{th} required to melt *c*-Si just beneath the PAI layer is ~90% of E_{melt} . The XTEM micrograph of the sample preamorphized with $1 \times 10^{15}/\text{cm}^2$, 5 keV Ge⁺ PAI is shown in Fig. 9. It is observed that the Ge⁺ PAI has created an amorphous layer ~116 Å thick. Figure 10 shows the simulated profiles of the implantation cascades of

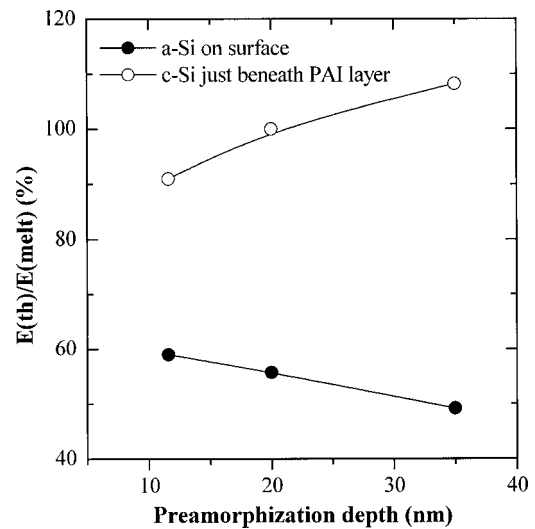


FIG. 8. Comparison of the simulated threshold fluence that is needed to melt an *a*-Si surface or *c*-Si just beneath the PAI layer to the threshold fluence that is required to melt *c*-Si at varying preamorphization depth.

$1 \times 10^{15}/\text{cm}^2$, 5 keV Ge⁺ PAI into *c*-Si. It can be seen that the boron profiles (both IMSIL and SIMS) are similar to that of the 10 keV Si⁺ PAI sample (as shown in Fig. 1), suggesting that this shallow amorphous layer is adequate to prevent significant channeling. Apparently, this boron profile is not completely contained within the amorphous layer created by the 5 keV Ge⁺ PAI. Thus, in this case, the excess interstitials generated by the 1 keV B⁺ implant (beyond the 116 Å amorphous layer) will also affect TED during subsequent annealing.²⁶

Figure 11 shows the simulated interstitial dose in the NEOR region (for the 5 keV Ge⁺ PAI sample) as a function of melt depth, taking into account the EI that were generated by the 1 keV B⁺ implant. It can be inferred that for melt depths greater than 245 Å, the interstitial dose in the NEOR region would be less than $5 \times 10^{12}/\text{cm}^2$. Hence it is expected that boron TED (especially enhanced diffusion arising from

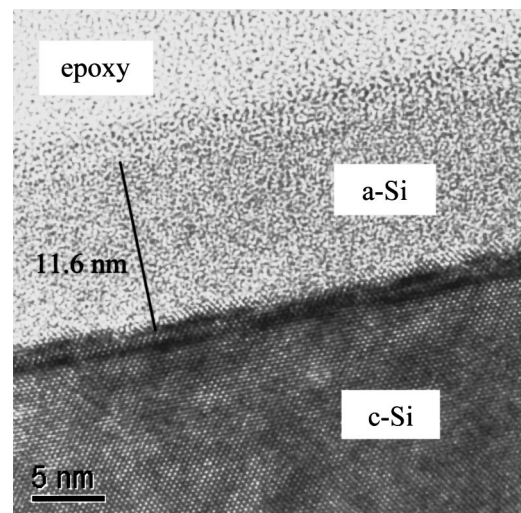


FIG. 9. XTEM micrograph of a sample that was preamorphized with $1 \times 10^{15}/\text{cm}^2$, 5 keV Ge⁺.

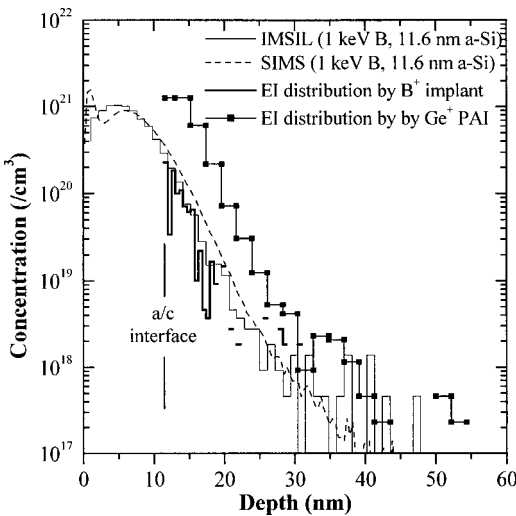


FIG. 10. SIMS profile of boron and simulated profiles of boron ions and excess interstitials that were generated by a 1 keV B⁺ implant and a 5 keV Ge⁺ PAI.

the dissolution of {311} defects) will be minimized for such melt depths. The SIMS profiles of boron (implanted into the Ge⁺ PAI sample) after LTP at 0.52 J/cm² and post-LTP RTA at 825 °C for 30 s are shown in Fig. 12. The maximum melt depth is estimated to be 280 Å, corresponding to an interstitial dose of $\sim 2.7 \times 10^{12}/\text{cm}^2$ in the NEOR region (refer to Fig. 11). Furthermore, it is observed that at a concentration of $1 \times 10^{18}/\text{cm}^3$, the junction has shifted only by ~ 30 Å during the post-LTP anneal. As the extent of boron diffusion is rather insignificant, the junction maintains its abruptness after the post-LTP anneal. This implies that TED can be suppressed by overmelting into the substrate, consistent with our hypothesis. The absence of TED also suggests that the amount of “quenched-in” interstitials in the recrystallized silicon (which can act as a source of interstitials) is negligible. This is probably due to the near-perfect liquid phase epitaxial regrowth of the melted layer, as shown in an earlier study.²⁷ The proposed mechanism on the control of boron

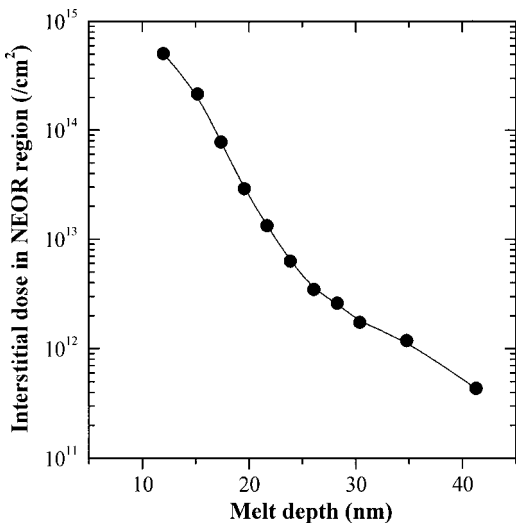


FIG. 11. Plot of the simulated interstitial dose in the NEOR region (for the 5 keV Ge⁺ PAI sample) as a function of melt depth.

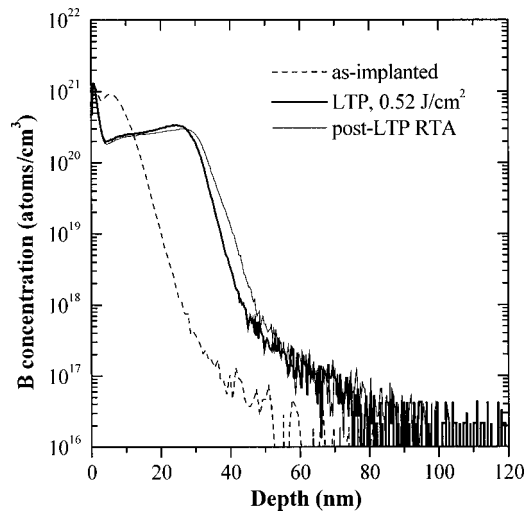


FIG. 12. SIMS profiles of boron (implanted into the Ge⁺ PAI sample) after LTP at 0.52 J/cm² and after a post-LTP RTA. Overmelting into the substrate eliminates boron TED.

TED during a post-LTP anneal is depicted in Fig. 6(b). It shows that for a shallower PAI layer, the melt front can easily penetrate into the NEOR region with a melt depth comparable to that of the deep PAI case, thus reducing the dose of interstitials that can contribute to TED during further annealing. A high resolution XTEM lattice image of the 5 keV Ge⁺ preamorphized sample after laser annealing at 0.52 J/cm² is shown in Fig. 13. It can be observed that the laser-regrown layer is virtually defect-free and does not contain any microtwins or stacking faults, as opposed to what might be expected in the absence of overmelting.¹³

IV. CONCLUSIONS

In summary, we have shown that although the amorphous layer in preamorphized silicon can be completely annealed by the nanosecond laser irradiation, the EOR damages were not sufficiently annealed. These EOR defects in turn

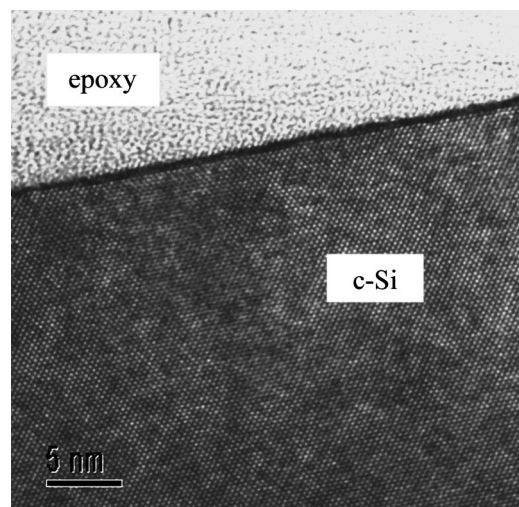


FIG. 13. High resolution XTEM lattice image of the 5 keV Ge⁺ preamorphized sample after laser annealing at 0.52 J/cm². The laser-regrown layer is virtually defect-free.

can cause boron TED during a post-LTP anneal. Since EOR damages cannot be avoided if a PAI is performed, the melt depth should be extended to beyond the amorphous layer to minimize the dose of interstitials in the NEOR region. We have demonstrated that by using a shallower PAI layer (where channeling is still prevented), the melt front can easily penetrate into the NEOR region with a melt depth that is comparable to that of the deep PAI case. In this way, even if the initial boron profile is not completely contained within the amorphous layer, TED can be significantly suppressed and the junction maintains its abruptness after the post-LTP anneal. It is found that overmelting into the substrate ensures a virtually defect-free regrown layer with a negligible amount of quenched-in interstitials.

ACKNOWLEDGMENTS

The authors are grateful to G. Hobler of Vienna University of Technology for the provision of IMSIL and H.-J. Gossmann for his support in running the simulations and helpful discussions. The authors would also like to thank Y. F. Lu, C. H. Tung, and R. Liu for their technical support. One of the authors (Y. F. Chong) acknowledges the National University of Singapore, National Science and Technology Board and Chartered Semiconductor Manufacturing Ltd. for his graduate scholarship.

¹E. C. Jones and E. Ishida, *Mater. Sci. Eng.*, **R**, **24**, 1 (1998).

²M. A. Foad, A. J. Murrell, E. J. H. Collart, G. de Cock, D. Jennings, and M. I. Current, *Mater. Res. Soc. Symp. Proc.* **568**, 55 (1999).

³E. J. H. Collart, K. Weemers, D. J. Gravesteijn, and J. G. M. van Berkum, *J. Vac. Sci. Technol. B* **16**, 280 (1998).

⁴A. Agarwal, H.-J. Gossmann, and A. T. Fiory, *J. Electron. Mater.* **28**, 1333 (1999).

⁵*The International Technology Roadmap for Semiconductors* (Semiconductor Industry Association, San Jose, 1999).

⁶P. A. Stolk, H.-J. Gossmann, D. J. Eaglesham, D. C. Jacobson, C. S.

Rafferty, G. H. Gilmer, M. Jaraiz, J. M. Poate, H. S. Luftman, and T. E. Haynes, *J. Appl. Phys.* **81**, 6031 (1997).

⁷A. Agarwal, H.-J. Gossmann, and D. J. Eaglesham, *Appl. Phys. Lett.* **74**, 2331 (1999).

⁸P. M. Fahey, P. B. Griffin, and J. D. Plummer, *Rev. Mod. Phys.* **61**, 289 (1989).

⁹A. Agarwal, H.-J. Gossmann, D. J. Eaglesham, L. Pelaz, D. C. Jacobson, T. E. Haynes, and Y. Erokhin, *Appl. Phys. Lett.* **71**, 3141 (1997).

¹⁰Y. F. Chong, K. L. Pey, A. T. S. Wee, A. See, L. Chan, Y. F. Lu, W. D. Song, and L. H. Chua, *Appl. Phys. Lett.* **76**, 3197 (2000).

¹¹S. Talwar, Y. Wang, and C. Gelatos, *Proc.-Electrochem. Soc.* **2000-9**, 95 (2000).

¹²M. O. Thompson, G. J. Galvin, J. W. Mayer, P. S. Peercy, J. M. Poate, D. C. Jacobson, A. G. Cullis, and N. G. Chew, *Phys. Rev. Lett.* **52**, 2360 (1984).

¹³K. S. Jones, H. Banisaukas, J. Glassberg, E. Andideh, C. Jasper, A. Hoover, A. Agarwal, and M. Rendon, *Appl. Phys. Lett.* **75**, 3659 (1999).

¹⁴H. Banisaukas, K. S. Jones, S. Talwar, D. F. Downey, and S. Falk, *Mater. Sci. Semicond. Process.* **4**, 339 (2001).

¹⁵K. S. Jones, L. H. Zhang, V. Krishnamoorthy, M. Law, D. S. Simons, P. Chi, L. Rubin, and R. G. Elliman, *Appl. Phys. Lett.* **68**, 2672 (1996).

¹⁶K. S. Jones, S. Prussin, and E. R. Weber, *Appl. Phys. A: Solids Surf.* **45**, 1 (1988).

¹⁷J. F. Ziegler, "SRIM2000," <http://www.srim.org>.

¹⁸G. Hobler, "IMSIL2000," TU Vienna, Austria, 2000.

¹⁹G. Hobler and C. S. Murthy, *Proceedings of the International Conference on Implantation Technology*, 2000, p. 209.

²⁰M. D. Giles, *J. Electrochem. Soc.* **138**, 1160 (1991).

²¹R. B. Fair, in *Impurity Doping Processes in Silicon*, edited by F. F. Y. Wang (North-Holland, New York, 1981), Chap. 7.

²²L. H. Zhang, K. S. Jones, P. H. Chi, and D. S. Simons, *Appl. Phys. Lett.* **67**, 2025 (1995).

²³L. C. Feldman, J. W. Mayer, and S. T. Picraux, *Materials Analysis by Ion Channeling: Submicron Crystallography* (Academic, New York, 1982), pp. 12–30.

²⁴D. J. Eaglesham, P. A. Stolk, H.-J. Gossmann, and J. M. Poate, *Appl. Phys. Lett.* **65**, 2305 (1994).

²⁵M. Uttormark, "Laser Melting Simulation Program-Version 3.0," University of Wisconsin-Madison.

²⁶H.-J. Gossmann (private communication).

²⁷Y. F. Chong, K. L. Pey, Y. F. Lu, A. T. S. Wee, T. Osipowicz, H. L. Seng, A. See, and J.-Y. Dai, *Appl. Phys. Lett.* **77**, 2994 (2000).